JCTC Journal of Chemical Theory and Computation

Molecular Thermodynamics of Methane Solvation in *tert*-Butanol−Water Mixtures

Maeng-Eun Lee and Nico F. A. Van der Vegt*

Max Planck Institute for Polymer Research, Ackermannweg 10, D-55128 Mainz, Germany

Received July 7, 2006

Abstract: We studied solvation structure and thermodynamics of methane in mixtures of *tert*-butanol and water using computer simulations. We show that for alcohol mole fractions below 20%, methane is preferentially solvated by hydrated alcohol clusters. Because methane expels water molecules from these clusters, a large endothermic solvent reorganization enthalpy occurs. This process is responsible for the experimentally observed maximum of the heat of methane solvation close to 5% alcohol in the mixture and contributes to a positive entropy change relative to solvation in pure water. Because the structural solvent reorganization enthalpy is enthalpy−entropy compensating, the methane solvation free energy is a smoothly varying function of the alcohol/water solution composition.

1. Introduction

Binary solvent mixtures are used in many applications in chemistry and biology. They are used for example as reaction media to control the rates of chemical reactions, as selective solvents where chemically different groups of a solvated solute each preferentially interact with one of the two solvent components and as media for studying the stability of biomolecules. Mixtures of organic solvents (but also cosolutes such as inorganic salts, sugars, urea, etc.) and water are of particular interest in biochemistry. Proteins are known to lose their stability in concentrated solutions of aqueous urea or guanidinium chloride,[1] whereas they may be stabilized at low temperatures (cryopreservation)[2] in aqueous solutions of disaccharides (e.g., trehalose) or polyols (e.g., ethylene glycol).[3,4] The atomic-scale mechanisms and their relation with physical-chemical properties of the solvent system are in many cases still incompletely understood and are the topic of ongoing discussion in the literature.[5−8]

In this paper we examine the thermodynamic process of methane dissolution in mixtures of water with *tert*-butyl alcohol. In this solvent system, the observed alcohol/water macromiscibility does not hold down to molecular length scales (microimmiscibility), and self-clustering of alcohol and water molecules occurs, in particular, in the water-rich composition regions.[9,10] Available experimental data show that the heat of methane solvation in this mixture passes through a maximum at approximately 5% alcohol in going from pure water to concentrated alcohol solutions (vide infra). Interestingly, this particular alcohol concentration corresponds to another maximum, which is that of the alcohol self-clustering.[10] It is the purpose of this paper to establish an atomic-scale picture that explains the nonmonotonic behavior of the methane solvation thermodynamics. In this context it is interesting to mention the recent study of Özal and Van der Vegt[11] who, based on molecular simulations, made calculations of solvent reorganization contributions to methane solvation entropies and enthalpies in mixtures of dimethyl sulfoxide and water.

2. Computational Details

2.1. ***tert*-Butanol, Water, and Methane Models.** We used the flexible six-site *tert*-butanol (TBA) model developed by Lee and Van der Vegt[10] (denoted LV-model from now on) in combination with the rigid three-site SPC water model.[12] TBA−TBA and TBA−water intermolecular interactions are modeled with a sum of Lennard-Jones (LJ) terms centered on the CH_3 (united atom methyl), C (central carbon), O (hydroxyl oxygen), and OW (water oxygen) interaction sites as well as Coulombic interactions between static partial electronic charges centered on the C, O, H (hydroxyl hydrogen), OW, and HW (water hydrogen) atoms. Geometric

* Corresponding author e-mail: vdervegt@mpip-mainz.mpg.de.

10.1021/ct600226h CCC: $37.00
Published on Web 12/02/2006

Table 1. Summary of MD Simulations of *tert*-Butanol/Water Mixtures[a]

x_{TBA}	N_{TBA}	N_{H2O}	t_{MD} (ns)	ϵ_{RF}	$V^{\#}$ (nm^3)	V (nm^3)
tert-Butanol(LV-Model)[10]/Water(SPC-Model)[12]						
0	0	1000	100	78.0	31.31	30.68
0.04	74	1776	150	64.8	65.83	65.29
0.06	105	1645	150	64.0	66.68	65.26
0.10	168	1512	100	50.7	72.48	71.73
0.20	275	1100	100	36.1	77.24	76.24
0.30	336	784	100	30.0	77.72	76.70
0.50	432	432	100	18.0	83.19	82.16
0.70	470	200	100	12.7	83.08	81.97
0.90	500	55	100	11.8	84.36	83.04
1.0	500	0	100	11.8	83.10	82.13
tert-Butanol(GROMOS-Model)[13]/Water(SPC-Model)						
0.06	105	1645	100	64.0	67.61	66.69
0.1	168	1512	100	50.7	73.76	72.82
0.2	275	1100	100	36.1	78.97	77.96
tert-Butanol(OPLS-Model)[14]/Water(SPC-Model)						
0.06	105	1645	100	64.0	67.46	66.56
0.10	168	1512	100	50.7	73.54	72.71
0.20	275	1100	100	36.1	78.24	77.51
tert-Butanol(OPLS-Model)/Water(TIP4P-Model)[15]						
0.06	105	1645	100	64.0	66.74	65.76
0.1	168	1512	100	50.7	72.89	71.78
0.2	275	1100	100	36.1	78.03	76.83

[a] The systems were simulated at constant pressure (1 atm) and temperature (298 K). x_{TBA}: TBA mole fraction; N_{TBA}: number of TBA molecules; N_{H2O}: number of water molecules; t_{MD}: total MD run time; ϵ_{RF}: reaction field dielectric permittivity; V: volume of the simulation box; $V^{\#}$: volume of the simulation box including 10 methane solutes.

mean mixing rules were used to describe LJ interactions between chemically different atom types/groups. For more details on the LV force field model we refer to ref 10. To assess model dependencies, we also used the GROMOS[13] and OPLS[14] *tert*-butanol models described in our previous work.[10] The GROMOS TBA-model was combined with the SPC water model, while the OPLS TBA-model was combined with the SPC and TIP4P[15] water models. In combination with the SPC water model, the latter two force fields produce too large alcohol−alcohol and water−water aggregation.[10] Although alternative force fields could possibly alleviate this effect, we use the GROMOS and OPLS force fields to get a better understanding of the relation between solvent structure and solute interaction thermodynamics. Methane was modeled as a united atom LJ-particle with parameters $\sigma = 0.373$ nm and $\epsilon = 1.247$ kJ/mol.[16] Geometric mean mixing rules were used to describe methane−solvent interactions.

2.2. Simulation Details. All simulations were performed using the GROMACS package.[17] Alcohol/water mixtures were studied at the *tert*-butanol mole fractions summarized in Table 1. Details on system sizes and simulation times are also given in Table 1. Geometries of all molecules were kept rigid by applying constraints to the interatomic distances within the molecules, using the SHAKE algorithm[18] with a relative geometric tolerance of 10^{-4}. A twin-range cutoff scheme with 0.8 and 1.4 nm cutoff radii was applied. The nonbonded interactions in the range between these radii were updated every fifth time step. The equations of motion were integrated using the leapfrog algorithm using a time step of 2 fs. A reaction field approximation was used to account for truncation of electrostatic forces beyond the long-range cutoff (1.4 nm). The reaction field relative dielectric permittivities are listed in Table 1. Constant pressure (1 atm) and temperature simulations were performed using the Nose−Hoover thermostat[19,20] and Rahman−Parrinello barostat[21,22] with coupling times $\tau_T = 1.5$ ps and $\tau_P = 2.5$ ps. Simulations were performed at three temperatures: 278, 298, and 318 K.

2.3. Solvation Free Energies, Enthalpies, and Entropies. The solvation free energies are calculated using the Widom test particle insertion method.[23] The solvation free energy ΔG is obtained by evaluating the expression[16]

$$\Delta G = -RT \ln[\langle V e^{-\psi/RT}\rangle_{NPT}/\langle V\rangle_{NPT}] \quad (1)$$

where ψ denotes the methane binding energy with the solvent, R denotes the gas constant, T is the temperature on the Kelvin scale, and V is the volume. The methane binding energy is evaluated at 125 000 random locations in each solvent configuration stored every 1 ps by summing overall methane−solvent LJ interactions. The angular brackets $\langle\cdots\rangle_{NPT}$ denote an averaging over constant pressure and temperature configurations of the solvent. In the simulation the averaging is performed over 100 ns simulation trajectories (Table 1).

The solvation entropy $\Delta S = -(\partial\Delta G/\partial T)_P$ is calculated using a finite-difference assumption

$$\Delta S(T) = -\frac{\Delta G(T+\Delta T) - \Delta G(T-\Delta T)}{2\Delta T} \quad (2)$$

where $T = 298$ K and $\Delta T = 20$ K in our calculations. In eq 2 it is assumed that the solvation heat capacity $\Delta c_P = T(\partial\Delta S/\partial T)_P$ is independent of temperature in the interval $2\Delta T$.[24] The solvation enthalpy (298 K) is obtained from the relation

$$\Delta H = \Delta G + T\Delta S \quad (3)$$

The statistical uncertainty of ΔG (eq 1) is smaller than 0.05 kJ/mol at all mixture compositions. The statistical uncertainty of $T\Delta S$ (eq 2) and ΔH (eq 3) is below 0.8 kJ/mol at all mixture compositions. Because eq 2 is only valid if the solvation heat capacity is constant over the selected temperature range, we decided to also determine ΔH and $T\Delta S$ with a direct method. In this method, performed at $T = 298$ K, the solvation enthalpy is determined by subtracting the potential energy of the solvent and the isolated solute from the solvated solute system potential energy. One then misses a term $P\Delta V$, which in condensed, liquid phases at ambient pressures usually is as small as 1−10 J/mol and can therefore safely be neglected. It is important, however, to subtract from the obtained potential energy difference a quantity $k_B T^2 \alpha_P$,[25] where α_P is the thermal expansion coefficient of the solvent. Having obtained ΔH by this direct approach, the solvation entropy can be obtained from the standard thermodynamic formula $T\Delta S = \Delta H - \Delta G$, where ΔG is obtained from eq 1. We used the direct approach by introducing ten methane solutes. Although a concentration

of ten solutes is above the solubility limit for all solvent mixtures, methane−methane interactions were observed to be negligible. We therefore assume that the methane solvation enthalpy with either one or ten methane solutes to be equal. The isobaric thermal expansion coefficient was obtained by performing, for each solvent composition, two additional 1 ns NPT simulations in which the temperature was changed ±10 K and the volume response was monitored; i.e. $\alpha_P \simeq (\ln[V_2/V_1]/[T_2 - T_1])_P$.

To better understand the enthalpy change we decompose this quantity in solute−solvent (ΔH_{uv}) and solvent−solvent enthalpy (ΔH_{vv}) changes, i.e.

$$\Delta H = \Delta H_{uv} + \Delta H_{vv} \tag{4}$$

The solute−solvent enthalpy change ΔH_{uv} is the sum of all solute−solvent pair interactions and was obtained by test-particle insertion[16]

$$\Delta H_{uv} = \frac{\langle V\psi e^{-\psi/RT}\rangle_{NPT}}{\langle Ve^{-\psi/RT}\rangle_{NPT}} \tag{5}$$

Calculations of ΔH_{uv} (eq 5) were all based on 100 ns sampling statistics with the systems summarized in Table 1. The enthalpy associated with changes of solvent−solvent interactions—ΔH_{vv} (the solvent reorganization enthalpy)—was obtained by means of eq 4 with ΔH obtained through eqs 1−3.

2.4. Solubility Data. We obtained the experimental methane solvation free energies, enthalpies, and entropies from the solubility data reported by Wang et al.[26] These data are reported in mole fraction methane (x_{CH_4}) in the solution at equilibrium with a methane pressure P at temperature T.[26] We use the Ben-Naim definition of the solvation process and the corresponding free energy change[27]

$$\Delta G = -RT \ln(\rho_{CH_4}/\rho^{ig}_{CH_4})_{eq} \tag{6}$$

where ρ_{CH_4} and $\rho^{ig}_{CH_4}$ are the methane molar densities in the solution and ideal gas phase, respectively. Both phases are at equilibrium as denoted by the subscript eq. In terms of the variables x_{CH_4}, P, and T used in ref 26 the solvation free energy (eq 6) becomes (assuming CH_4 is present at infinite dilution in the binary solvent)

$$\Delta G = RT \ln K_H - RT \ln (RT\rho_{solv}) \tag{7}$$

where ρ_{solv} is the molar density of the pure solvent phase (i.e., the alcohol/water mixture) and $K_H = \lim_{x_{CH4}\to 0}(P/x_{CH_4})$ the Henry coefficient. Experimental information on ρ_{solv} was obtained from ref 28. We note that K_H is usually expressed in units of atmospheres in which case $RT\ \rho_{solv}$ should also be expressed in these units. Wang et al.[26] reported methane solubility data at 283.15 K, 288.15, 293.15, and 298.15 K. By applying the finite difference method (eq 2) to the free energies obtained from eq 6 at 288.15 and 298.15 K we obtain the experimental solvation entropies at 293.15 K. The experimental solvation enthalpies at 293.15 K are next obtained from eq 3 using the solvation entropies together with the experimental solvation free energies at 293.15 K. Note that the so-derived solvation enthalpies and entropies all apply at a temperature 5 K below the temperature (298 K) used in our simulations. The discrepancy due to this difference in temperature we estimate based on the experimental heat capacity change Δc_P (142 J/mol K) of solvating methane in water at 298 K.[29] Assuming this value remains constant in the 5 K temperature range results in a 0.7 kJ/mol difference in ΔH and $T\Delta S$ (i.e., the values being 0.7 kJ/mol higher at the higher temperature).

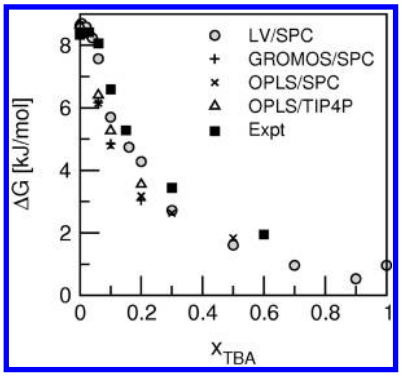

Figure 1. (a) Methane solvation free energy ΔG (eq 1) presented versus the *tert*-butanol mole fraction in aqueous *tert*-butanol solvent: squares, experimental data;[26] circles, the LV/SPC model; plusses, the GROMOS/SPC model; crosses, the OPLS/SPC model; and triangles, the OPLS/TIP4P model.

3. Results and Discussion

3.1. Free Energy of Methane Solvation. Figure 1 shows the methane solvation free energies at 298 K and 1 atm presented versus the alcohol mole fraction x_{TBA} of the solution. Transfer of the methane solute from pure water to pure *tert*-butanol causes the free energy to decrease with approximately 8 kJ/mol corresponding to a 25-fold increase of the methane solubility at 298 K. The shape of the curve ($\partial\Delta G/\partial x_{TBA} < 0$) indicates[16,27] that methane in TBA/water solution preferentially interacts with the alcohol molecules. Four TBA/water force field combinations have been used to calculate the ΔG data in Figure 1: LV/SPC, GROMOS/SPC, OPLS/SPC, and OPLS/TIP4P. The best agreement with the experimental data (squares) is observed for the LV/SPC model; the calculated data match the experimental values for x_{TBA} up to 0.06; at larger alcohol mole fractions the free energies are slightly underestimated by the model. For x_{TBA} up to 0.2, the GROMOS/SPC and OPLS/SPC models result in almost identical methane solvation free energies, which are however lower than the experimental and LV/SPC values. The ΔG values obtained based on the OPLS/TIP4P solvent model are slightly improved over those values obtained based on the corresponding OPLS/SPC model but are still systematically below the experimental and LV/SPC data. Table 3 summarizes the experimental[26] and calculated (LV/SPC model) thermodynamic data.

3.2. Preferential Solvation. Figure 2 shows methane−solvent radial distribution functions $g(r)$. The radial distribution functions (RDFs) were obtained from simulations including ten methane solutes in the systems summarized in Table 1. The left panel in Figure 2 shows the methane−TBA (methyl) RDF at TBA mole fractions 0.06, 0.1, and 0.2. The right panel shows the methane−water (oxygen)

Table 2. First Shell Coordination Numbers and Excess First Shell Coordination Numbers (in Parentheses) for Methane−TBA and Methane−Water[a]

x_{TBA}	methane−TBA	methane−water
tert-Butanol (LV-Model)/Water (SPC-Model)		
0.04	3.3(1.0)	13.7(−3.3)
0.06	5.6(2.3)	9.8(−5.7)
0.1	7.9(3.0)	5.9(−7.2)
0.2	9.5(2.1)	3.3(−5.7)
0.3	10.1(1.1)	2.2(−4.1)
0.5	10.7(−0.2)	1.2(−2.1)
0.7	11.0(−0.9)	0.6(−0.9)
0.9	11.1(−1.3)	0.2(−0.2)
tert-Butanol (GROMOS-Model)/Water(SPC-Model)		
0.06	7.0(3.8)	7.2(−9.3)
0.1	8.4(3.8)	4.7(−9.2)
0.2	9.7(2.6)	2.5(−7.0)
tert-Butanol (OPLS-Model)/Water(SPC-Model)		
0.06	6.8(3.6)	7.5(−9.0)
0.1	8.4(3.8)	4.8(−9.1)
0.2	9.7(2.5)	2.7(−6.9)
tert-Butanol (OPLS-Model)/Water(TIP4P-Model)		
0.06	7.5(4.3)	6.1(−10.7)
0.1	9.1(4.1)	4.8(−10.1)
0.2	10.6(2.9)	2.4(−7.9)

[a] The number of TBA and water molecules in the first shell was computed by integrating, respectively, the methane−CH_3 and methane−water−oxygen RDFs up to 0.53 nm.

Table 3. Thermodynamic Data for Methane Solvation (298 K, 1 atm) in TBA/Water Mixtures[a]

x_{TBA}	ΔG_{exp}	ΔG_{sim}	ΔH_{exp}	ΔH_{sim}	$T\Delta S_{exp}$	$T\Delta S_{sim}$
0.0	8.3	8.6	−11.5	−2.6	−19.8	−11.2
0.01	8.4	8.6	−8.4	−0.7	−16.6	−9.2
0.03	8.4		−7.6		−16.0	
0.04		8.2		2.9		−5.3
0.06	8.1	7.6	4.6	4.5	−3.5	−3.1
0.1	6.6	5.7	3.9	3.6	−2.7	−2.4
0.15	5.3	4.7	3.5	1.1	−1.8	−3.6
0.2		4.3		0.2		−4.1
0.3	3.4	2.7	0.7	−1.0	−2.7	−3.7
0.5		1.6		−2.9		−4.5
0.6	2.0		0.4		−1.6	
0.7		1.0		−2.8		−3.8
0.9		0.5		−3.5		−4.0
1		1.0		−1.9		−2.9

[a] The experimental data (denoted with subscript exp) were obtained from ref 26 (see section 2.4). The data calculated based on simulations (denoted with subscript sim) were obtained with the LV/SPC model[10] using test-particle insertions and finite temperature differences (eqs 1−3). Units are kJ/mol.

RDFs at the same solution compositions. Methane preferentially interacts with TBA-methyl groups. All RDFs (left panel) show a first peak at 0.4 nm followed by a second and third peak superimposed on an exponential type decay of the RDF toward unity. The limiting value (RDF = 1) is reached at approximately 1.5 nm with the LV/SPC model, while with all other models box sizes are too small to observe this limit. For the methane−water RDFs (right panel) the physical picture is reversed: a first peak is observed at

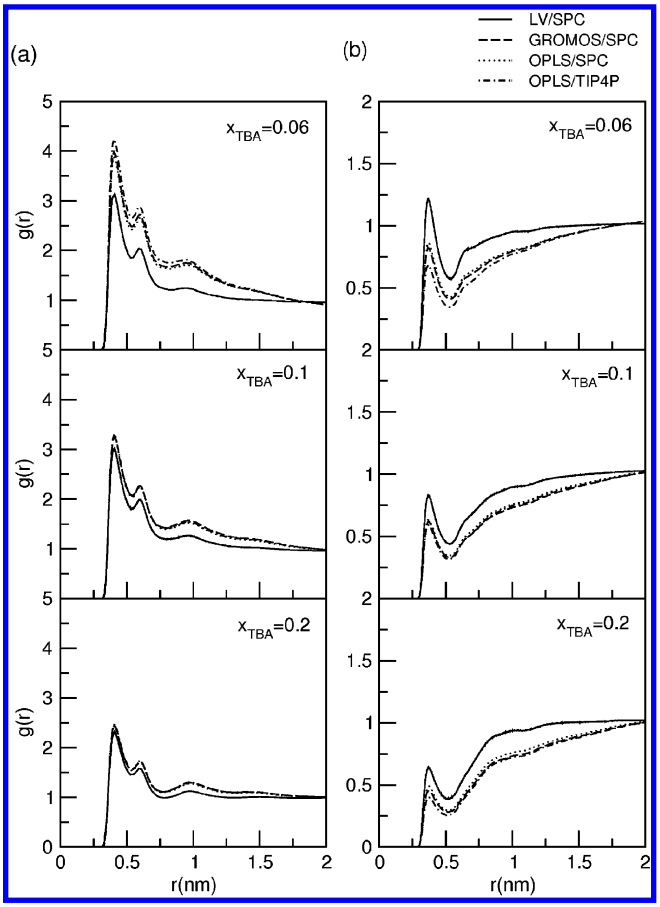

Figure 2. Solute (CH_4)−solvent radial distribution functions $g(r)$ versus the distance r at $x_{TBA} = 0.06$, $x_{TBA} = 0.1$, and $x_{TBA} = 0.2$ *tert*-butanol mole fractions: (a) methane−*tert*-butanol (methyl groups), (b) methane−water (oxygen). Solid line, LV/SPC model; dashed, the GROMOS/SPC model; dotted, the OPLS/SPC model; dashed-dotted, the OPLS/TIP4P model.

0.36 nm, followed by a water depletion region (RDF<1) up to 1.5 nm for the LV/SPC model; with all other models the limiting value RDF = 1 is not reached for distances up to 2 nm. First shell coordination numbers obtained by integrating the RDFs up to the first minimum are summarized in Table 2.

To quantify the excess amount of TBA and water vicinal to the methane solute we calculated methane−solvent excess coordination numbers N_j^{ex} defined as

$$N_j^{ex} = \rho_j \int_0^R [g_{Sj}(r) - 1] 4\pi r^2 dr \qquad (8)$$

In eq 8, ρ_j denotes the solvent component number density, $g_{Sj}(r)$ denotes the solute (CH_4)−solvent RDF, and R is an integration cutoff, which we chose to be 1 nm. Figure 3a,b shows the methane−TBA and methane−water excess coordination numbers, respectively. The CH_4−TBA excess coordination number (LV/SPC model) goes through a maximum at $x_{TBA} = 0.1$, while the CH_4−water excess coordination number goes through a minimum at this solvent composition. This behavior correlates with a maximum observed in the TBA−TBA Kirkwood-Buff integral at the same solvent composition.[10] With the GROMOS and OPLS models excess coordination numbers are found that exceed those obtained with the LV/SPC model by 50−60%.

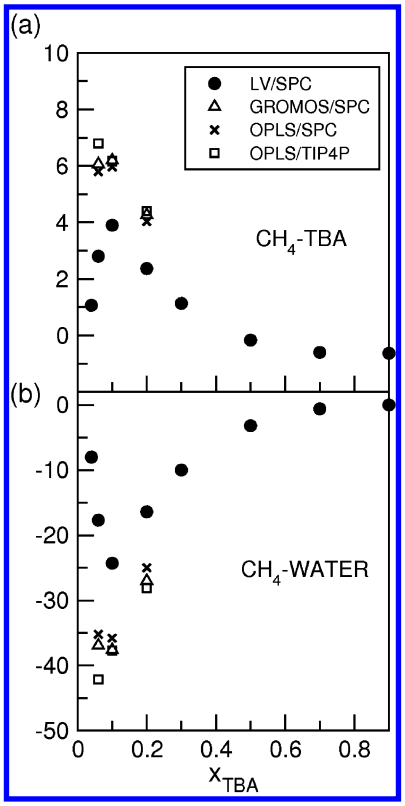

Figure 3. (a) Excess coordination numbers (eq 8 with R = 1 nm) for methane and *tert*-butanol obtained with the LV/SPC model (black circle), the GROMOS/SPC model (triangle), the OPLS/SPC model (cross), and the OPLS/TIP4P model (square). (b) Excess coordination number (eq 8 with R = 1 nm) for methane and water (oxygen).

3.3. Methane Solvation Enthalpy and Entropy. Figure 4a,b shows the methane solvation enthalpies and entropies versus the alcohol mole fraction of the solution. Interestingly, these curves are nonmonotonic in contrast to the solvation free energy (Figure 1). The experimental data (squares) indicate a rapid increase of ΔH with x_{TBA}. Methane solvation is exothermic in water but switches to endothermic between 3 and 6 mol % TBA in the solution. A maximum in ΔH is observed at $x_{TBA} = 0.06$. The methane solvation enthalpy decreases with a further increase of x_{TBA}. The methane solvation entropy rapidly increases up to $x_{TBA} \approx 0.1$ and then remains practically constant. With the LV/SPC model the experimental enthalpy curve and the transition from exo- to endothermic solvation are qualitatively reproduced. The maximum is predicted at the appropriate alcohol concentration and is almost quantitatively reproduced. At higher TBA mole fractions ($x_{TBA} > 0.06$) the solvation enthalpies are underestimated, while at higher alcohol dilution ($x_{TBA} < 0.06$) the solvation enthalpies are overestimated (see also Table 3). The same observations apply for the solvation entropies. Note that in water ($x_{TBA} = 0$) the methane solvation enthalpy and entropy are significantly overestimated. This is caused by a too large thermal expansion coefficient of the SPC water model resulting in a too large solvent reorganization enthalpy.[11,25] Based on the GROMOS and OPLS models (right panel in Figure 4) the solvation enthalpies and entropies are less well reproduced; although the downward trend of the enthalpy agrees with the experimental data, the sign is wrong, indicating that a significant, positive enthalpy contribution is missing.

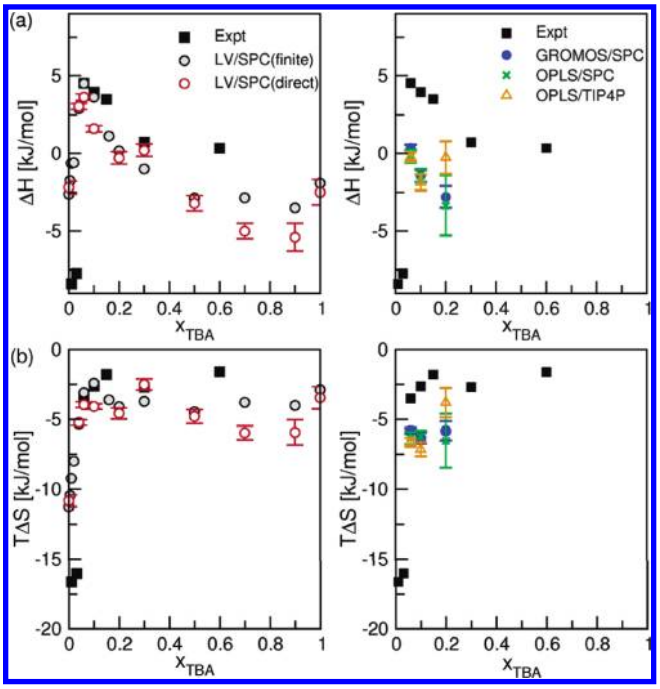

Figure 4. (a) Methane solvation enthalpies ΔH presented versus the *tert*-butanol mole fraction x_{TBA} in the solvent and (b) methane solvation entropies $T\Delta S$ versus x_{TBA}. For the LV/SPC model, solvation entropies and enthalpies obtained by finite temperature difference are shown as gray circles; the solvation enthalpies and entropies, obtained through the direct difference route, are shown as red circles. For the GROMOS and OPLS models (right panel), the solvation enthalpies and entropies were obtained through the direct difference route.

Table 4. Methane Solvation Enthalpy $(\Delta H)_{direct}$ Obtained from Taking Direct Energy Differences (cf. Section 2.2), Solvation Enthalpy $(\Delta H)_{FT}$ Obtained by Finite-Temperature (FT) Differences (Eqs 1−3), Structural Solvent Reorganization Energy (ΔH_{vv}), and Solute−Solvent Binding Energy (ΔH_{uv}) in TBA/Water (298 K, 1 atm) Obtained with the LV/SPC Model[10] [a]

x_{TBA}	$RT^2\alpha_P$	$(\Delta H)_{direct}$	$(\Delta H)_{FT}$	ΔH_{vv}	ΔH_{uv}
0.0	0.54	−2.2 ± 0.4	−2.6	11.2	−13.8
0.01			−0.7	12.7	−13.4
0.04	0.71	3.0 ± 0.2	2.9	16.2	−13.3
0.06	0.76	3.6 ± 0.2	4.5	17.7	−13.2
0.1	0.83	1.6	3.6	16.6	−13.0
0.15			1.1	14.1	−13.0
0.2	0.86	−0.3 ± 0.4	0.2	13.1	−12.9
0.3	0.88	0.2 ± 0.4	−1.0	12.0	−13.0
0.5	0.86	−3.2 ± 0.5	−2.9	10.2	−13.1
0.7	0.87	−5.0 ± 0.5	−2.8	10.2	−13.0
0.9	0.86	−5.4 ± 0.9	−3.5	9.5	−13.0
1	0.87	−2.5 ± 0.8	−1.9	11.0	−12.9

[a] Note that ΔH_{uv} depends only weakly on the TBA/water solvent composition, while ΔH_{vv} determines the compositional dependence of ΔH. Units are kJ/mol.

Table 4 and Figure 5 show the contributions of the solvent reorganization enthalpy (cf. eq 4) to the overall solvation enthalpy. Inspection of these data (LV-model) shows that

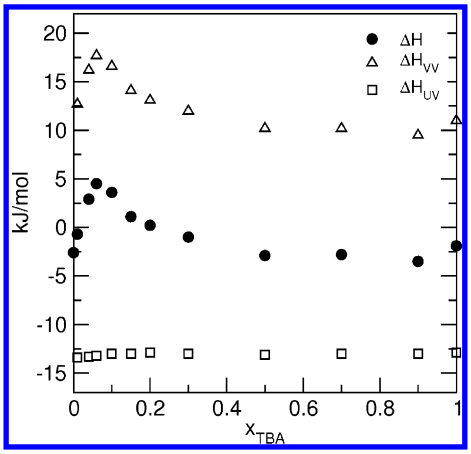

Figure 5. Methane solvation enthalpies ΔH (black circles), obtained from finite temperature differences (eqs 1−3), and contributions of solute−solvent interactions ΔH_{uv} (squares) (eq 5) and solvent reorganization enthalpy ΔH_{vv} (triangles) (eq 4) for the LV/SPC model. Note that changes of ΔH with the alcohol/water solution composition are almost exclusively determined by the enthalpy change ΔH_{vv} of structural solvent reorganization.

Table 5. Contributions of Water−Water, TBA−TBA, and TBA−Water Interactions to the Solvent Reorganization Enthalpy ΔH_{vv} at 298 K and 1 atm[a]

x_{TBA}	$\Delta H_{H_2O-H_2O}$	$\Delta H_{TBA-TBA}$	ΔH_{TBA-H_2O}
	LV/SPC		
0.04	80 ± 3	−16 ± 9	114 ± 17
0.06	−5 ± 13	−35 ± 8	219 ± 19
0.1	−41 ± 22	−11 ± 13	210 ± 31
0.2	−54 ± 42	14 ± 29	189 ± 64
0.3	13 ± 42	91 ± 35	31 ± 72
0.5	−63 ± 36	46 ± 33	151 ± 63
0.7	−21 ± 37	86 ± 36	63 ± 68
0.9	0 ± 8	131 ± 14	2 ± 18
	GROMOS/SPC		
0.06	−13 ± 19	−2 ± 11	158 ± 25
0.1	−89 ± 31	−27 ± 19	242 ± 40
0.2	−53 ± 61	33 ± 43	134 ± 95
	OPLS/SPC		
0.06	−18 ± 35	−10 ± 26	164 ± 50
0.1	−43 ± 55	−1 ± 44	171 ± 91
0.2	−138 ± 162	−63 ± 137	311 ± 272
	OPLS/TIP4P		
0.06	−63 ± 31	−33 ± 29	231 ± 48
0.1	−87 ± 60	−27 ± 44	238 ± 92
0.2	95 ± 100	165 ± 85	−119 ± 329

[a] The contributions were obtained by subtracting the potential energy components of a pure solvent box from the respective energy components of boxes including ten methane solutes. Averaging was performed over 100 ns simulations (Table 1). The error bars were obtained by block averaging. Units are kJ/mol.

the shape of the enthalpy curve is entirely determined by the solvent reorganization enthalpy ΔH_{vv}; the solute−solvent enthalpy ΔH_{uv} changes only little with the solution composition (Figure 5). Further separation of ΔH_{vv} in Table 5 shows that the largest contribution to the enthalpy maximum observed in Figures 4a and 5 results from changes in *tert*-butanol−water interactions. With the GROMOS/SPC, OPLS/SPC, and OPLS/TIP4P models changes in *tert*-butanol−water interactions result in a positive enthalpy contribution too, but these are smaller or compensated by a negative enthalpy contribution of water−water interactions resulting in a larger discrepancy with the experimental data (Figure 4a).

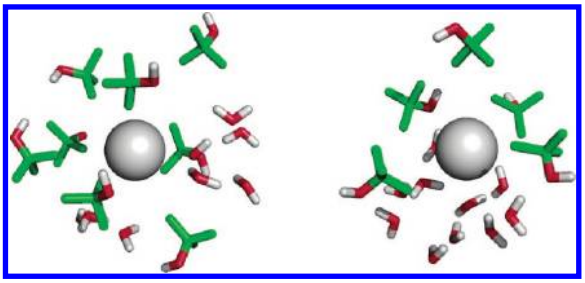

Figure 6. Simulation snapshots (LV/SPC model) showing the composition of the first solvation shell of methane (gray sphere) at $x_{TBA} = 0.1$. All solvent molecules within 0.6 nm from the central methane solute are shown. Color code: oxygen (red), hydrogen (white), and carbon/methyl (green). Alcohol molecules preferentially solvating methane lose hydration waters.

The solvation entropy (Figure 4b) follows the trend of the enthalpy (Figure 4a); however, there is no clear maximum. We note here that the solvent reorganization enthalpy occurs as a contribution $\Delta H_{vv}/T$ in the entropy,[30,31,11] hence it is not surprising that the discrepancies in ΔH, observed with the GROMOS and OPLS models, occur in the entropy changes too.

3.4. Discussion. Mixtures of *tert*-butanol and water exhibit significant alcohol clustering at low alcohol contents. The largest excess alcohol−alcohol aggregation occurs around 10 mol % alcohol in the mixture.[10] From Figures 2 and 3 it is evident that methane is solvated by these hydrated clusters. Snapshots of this situation are shown in Figure 6 and include only the solvent molecules in the first solvation shell. A key difference between the LV model, on the one hand, and the GROMOS and OPLS models, on the other hand, is that the LV model has been parametrized to reproduce the experimental alcohol and water activities in the mixture.[10] Alcohol clusters in the water-rich composition regions remain sufficiently hydrated to keep the system miscible. Water molecules are however expelled from the alcohol clusters by the introduction of methane. As shown in Table 5, this leads to a significant enthalpy increase due to disruption of alcohol−water cohesive interactions. The endothermic heat of methane dissolution around $x_{TBA} = 0.1$ (Figure 4) is therefore explained by the atomic-scale picture where methane sticks to alcohol clusters and expels hydration water.

The procedure of validating the solvation enthalpies and entropies seems to provide better insight in the accuracy of solvent models in general since the discrepancies observed in these quantities (Figure 4, right panel) are larger than in the solvation free energy (Figure 1). A similar observation was made by Weerasinghe and Smith,[32] who found that free energies of cavity formation in aqueous urea systems are independent of the extent of urea aggregation, while preferential interaction is intimately related to the solution mixture structure. As we pointed out above, the solvent reorganization enthalpy ΔH_{vv} is always exactly enthalpy−entropy compensating, and, therefore, it does not influence the free energy change.[30,31,11] The free energy change can therefore be perfectly reproduced, while its enthalpic and entropic components are

not. The solvation enthalpy, which contains a contribution ΔH_{vv}, and entropy, which contains a contribution $\Delta H_{vv}/T$, are strongly influenced by changes in solvent−solvent interactions and in that sense sensitively probe the quality of the force field describing the aqueous/organic solvent mixture.

4. Conclusions

We performed atomistic computer simulations of methane solvated in mixtures of *tert*-butanol and water. In addition to aspects of preferential methane solvation in terms of radial distribution functions and excess coordination of solvent components, we calculated the methane solvation free energy, enthalpy, and entropy based on four force field models available in the literature. Since preferential solvation of solutes by cosolvent or water molecules is likely to be coupled to aspects of cosolvent and water clustering in the solvent mixture, we used the Lee and Van der Vegt (LV) force field,[10] which was parametrized to reproduce the solvent Kirkwood-Buff integrals. We find that the enthalpy and entropy changes of methane insertion are very sensitive to changes of solvent−solvent interactions and therefore accurately probe the quality of the force fields for this solvent mixture. In particular, at high alcohol dilution, methane sticks to hydrated alcohol clusters and expels alcohol hydration water. This process is responsible for an endothermic heat of methane solvation (as opposed to exothermic solvation in pure water) and an increase of the solvation entropy.

References

(1) Tanford, C. *Adv. Protein Chem.* **1970**, *24*, 1.

(2) Carpenter, J. F.; Crowe, J. H. *Cryobiology* **1988**, *25*, 459.

(3) Xie, G. F.; Timasheff, S. N. *Biophys. Chem.* **1997**, *64*, 25.

(4) Wang, G. M.; Haymet, A. D. J. *J. Phys. Chem. B* **1998**, *102*, 5341.

(5) Lins, R. D.; Pereira, C. S.; Hünenberger, P. H. *Proteins* **2004**, *55*, 177.

(6) Shimizu, S.; Chan, H. S. *Proteins* **2002**, *49*, 560.

(7) Bennion, B. J.; Daggett, V. *Proc. Natl. Acad. Sci. U.S.A.* **2003**, *125*, 1950.

(8) Lee, M. E.; Van der Vegt, N. F. A. *J. Am. Chem. Soc.* **2006**, *128*, 4948.

(9) Matteoli, E.; Lepori, L. *J. Chem. Phys.* **1984**, *80*, 2856.

(10) Lee, M. E.; Van der Vegt, N. F. A. *J. Chem. Phys.* **2005**, *122*, 114509.

(11) Özal, T. A.; Van der Vegt, N. F. A. *J. Phys. Chem. B* **2006**, *110*, 12104.

(12) Berendsen, H. J. C.; Postma, J. P. M.; Van Gunsteren, W. F.; Hermans, J. in *Intermolecular Forces*; Pullman, B. Ed.; Reidel: Dordrecht, 1981; pp 331−342.

(13) Oostenbrink, C.; Villa, A.; Mark, A. E.; Van Gunsteren, W. F. *J. Comput. Chem.* **2004**, *25*, 1656.

(14) Jorgensen, W. L. *J. Phys. Chem.* **1986**, *90*, 1276.

(15) Jorgensen, W. L.; Chandrasekhar, J.; Madura, J. D.; Impey, R. W.; Klein, M. L. *J. Chem. Phys.* **1983**, 926.

(16) Van der Vegt, N. F. A.; Van Gunsteren, W. F. *J. Phys. Chem. B* **2004**, *108*, 1056.

(17) Van der Spoel, D.; Lindahl, E.; Hess, B.; Groenhof, G.; Mark, A. E.; Berendsen, H. J. C. *J. Comput. Chem.* **2005**, *26*, 1701.

(18) Ryckaert, J. P.; Ciccotti, G.; Berendsen, H. J. C. *J. Comput. Phys.* **1977**, *23*, 327.

(19) Nosé, S. *Mol. Phys.* **1984**, *52*, 255.

(20) Hoover, W. G. *Phys. Rev. A* **1985**, *31*, 1695.

(21) Rahman, A.; Parrinello, M. *J. Appl. Phys.* **1981**, *52*, 7182.

(22) Nosé, S.; Klein, M. L. *Mol. Phys.* **1983**, *50*, 1055.

(23) Widom, B. *J. Chem. Phys.* **1963**, *39*, 2808.

(24) Smith, D. E.; Haymet, A. D. J. *J. Chem. Phys.* **1993**, *98*, 6445.

(25) Hess, B.; Van der Vegt, N. F. A. *J. Phys. Chem. B* **2006**, *110*, 17616.

(26) Wang, Y.; Han, B.; Yan, H.; Liu, R. *Thermochim. Acta* **1995**, *253*, 327.

(27) Ben-Naim, A. *Molecular Theory of Solutions*; Oxford University Press: New York, 2006.

(28) Nakanishi, K.; Kato, N.; Maruyama, M. *J. Phys. Chem.* **1967**, *71*, 814.

(29) Makhatadze, G. I.; Privalov, P. L. *J. Mol. Biol.* **1993**, *22*, 639.

(30) Yu, H. A.; Karplus, M. *J. Chem. Phys.* **1988**, *89*, 2366.

(31) Van der Vegt, N. F. A.; Trzesniak, D.; Kasumaj, B.; Van, Gunsteren, W. F. *Chem. Phys. Chem.* **2004**, *5*, 144.

(32) Weerasinghe, S.; Smith, P. E. *J. Chem. Phys.* **2003**, *118*, 5901.

CT600226H